

Topology of the mesoscale connectome of the mouse brain

Pascal Grange

Xi'an Jiaotong-Liverpool University, Department of Mathematical Sciences, Suzhou, China

Pascal.Grange@xjtlu.edu.cn

Abstract

The wiring diagram of the mouse brain has recently been mapped at a mesoscopic scale in the Allen Mouse Brain Connectivity Atlas. Axonal projections from brain regions were traced using green fluorescent proteins. The resulting data were registered to a common three-dimensional reference space. They yielded a matrix of connection strengths between 213 brain regions. Global features such as closed loops formed by connections of similar intensity can be inferred using tools from persistent homology. In this paper the wiring diagram of the mouse brain is mapped to a simplicial complex (filtered by connection strength), and generators of the first homology group are computed. Some regions, including nucleus accumbens, are connected to the entire brain by loops. Thousands of loops go through the isocortex, the striatum and the thalamus. On the other hand, medulla is the only major brain compartment that contains more than 100 loops.

1 Introduction

The Allen Mouse Brain Connectivity Atlas [1] has filled a major gap in the knowledge of neuroanatomy by providing a brain-wide map of the connectome of the mouse brain. Adeno-associated viral vectors expressing enhanced green fluorescent protein were injected into the mouse brain, allowing to trace axonal projections. The scale of these experiments is mesoscopic [2], in the sense that injections target groups of neurons belonging to brain regions assumed to be homogeneous. The microscopic scale would correspond to mapping individual synapses where neurons make contact. The resulting three-dimensional fluorescent traces were registered to brain regions defined in the hierarchical Allen Reference Atlas [3].

These results allowed the construction of the first inter-region connectivity model of the mouse brain. It takes the form of a connectivity matrix, whose rows and columns correspond to a brain region, and whose entries model the connection strengths between pairs of regions defined by classical neuroanatomy. The derivation of the entries of the connectivity matrix assumed homogeneity of brain regions and additivity of connection strengths. Projection densities correspond to axons highlighted by tracers, hence the projection densities from several different sources sum to produce projection density in a given region. This additivity assumption was used to address experimental data in which an injection of viral tracer infected several neighbouring brain regions.

The construction of the model from injection data (possibly infecting several regions for each injection) assumes that projections are homogeneous in each region, and that projections from different sources add to produce projection density to a given region. The entries of the connectivity matrix were observed to span a 10^5 -fold range, and are approximately fit by a log-normal distribution.

The connectivity matrix is naturally mapped to a graph that models the wiring diagram of the mouse brain. Some features of the wiring diagram such as node degree and clustering coefficient have been observed to be reproduced by scale-free networks [4] and small-world networks [5], but none of these models was found to fit all observed features of the wiring diagram. This begs for further modelling taking into account the global properties of the connectivity map, together with the large range of intensities mapped by connection strengths.

On the other hand, the recent computational developments of algebraic topology [6–9] have given rise to spectacular applications to data analysis in biological sciences, including obstructions to phylogeny in viral evolution [10], and brain networks and neural correlations [11–15]. In this paper we will apply techniques from algebraic topology, a branch of mathematics characterizing properties of spaces that are invariant by continuous deformation, to work out global properties of the wiring diagram of the mouse brain.

We will first review the presentation of the Allen Mouse Brain Connectivity Atlas in the form of a matrix modelling connection strengths between brain regions. We will define a mapping from these data to a filtered simplicial complex and explain why the generators of the first homology group are in one-to-one correspondence with closed loops in the mesoscale connectome. The anatomy of these loops will then be analysed by grouping loops according to the major brain compartments they intersect. Moreover, we will compare the fraction of the brain reached from each region by loops, to the fraction reached by direct connections encoded in the connectivity matrix.

2 Materials and methods

2.1 Connectivity strengths in the mouse brain, local and global properties

Each image series in the Allen Mouse Connectivity Atlas corresponds to an injection of tracer, followed by sectioning and and imaging of the brain¹. In [1], registered data from 469 image series were combined in order to estimate an inter-region connectivity matrix, presented in matrix form²:

$$C(r, r') = \{\text{connection strength from region labelled } r \text{ to region labelled } r'\}, \quad 1 \leq r, r' \leq R. \quad (1)$$

The size of this connectivity matrix is $R = 213$, and each of the indices in $\{1, \dots, R\}$ corresponds to a brain region, defined in the Allen Reference Atlas (ARA, [3, 16]).

The connectivity matrix captures the local structure of the connectome at mesoscopic scale, as it estimates the strength of direct connections from a region to other regions. To capture global features of the connectome, we would like to identify closed circuits constructed from these connections. Algebraic topology formalises this notion: an irreducible closed loop in a topological space (a loop that cannot be shrunk to a point by continuous deformations) is a loop that is not the boundary of a disc in the topological space. It is therefore a one-dimensional cycle that is not the boundary of a two-dimensional object. The family of such objects in a topological space is invariant by continuous deformation, and has a group structure. It is called the first homology group of the topological space, and denoted by H_1 .

If we repeat this reasoning in dimension zero, we obtain the more familiar notion of connected component: elements of H_0 are zero-dimensional objects that cannot be joined by a path drawn on the topological space. They correspond to distinct connected components. More generally, the

¹ © 2014 Allen Institute for Brain Science. Allen Connectivity Atlas. Available from: <http://connectivity.brain-map.org/.org>

²The entries of the matrix C correspond to the left-hand side of Fig. 3 in [1].

elements of the homology group H_k are objects of dimension k that are not boundaries of $(k + 1)$ -dimensional objects in a topological space, and therefore formalise the notion of hole. Moreover, the algebraic structure of homology groups allows us to count independent objects in each of them: the number of generators of the homology group H_k is called the k -th Betti number and denoted by b_k . The Betti numbers b_0 and b_1 are the number of connected components and the number of independent loops respectively.

2.2 Mapping the matrix of connection strengths to a filtered simplicial complex

The connectivity matrix C is not symmetric, because projections from a given brain region to other brain regions are oriented (just as axons are). Let us map the connectivity matrix to a weighted graph with R vertices corresponding to brain regions, and weighted edges corresponding to the entries of the connectivity matrix. Edges with two different orientations and different weights can exist between pairs of vertices. Let us apply a decreasing function to the entries of the connectivity matrix and define for instance:

$$d(r, s) = -\log(C(r, s) + \epsilon), \quad (2)$$

where ϵ is a positive regulator chosen to be smaller than the minimum connection strength, so that entries of d are bounded. The families of loops worked out in this paper do not depend on the choice of ϵ (in practice we took $\epsilon = 0.01\min_{r,s}C(r, s)$, resulting in a maximum entry of 42 for d). This operation results in an approximately normal distribution of entries in the matrix d . The quantity $d(r, s)$ has been observed in [1] to be positively correlated to the spatial distance between region labelled r and region labelled s . However, the entries of d are not quite distances because d is not symmetric.

We propose to map brain regions to a graph with $2R$ vertices as follows. Each brain region, labelled r , is mapped to a pair of vertices (s_r, t_r) , where s_r represents the sources of action potentials (the axons of the cell bodies in the region, that conduct axon potentials), and t_r the targets of action potentials (the dendrites in the region, that receive action potentials). An edge is drawn between vertices t_r and s_r for each r in $\{1, \dots, R\}$. With this doubling prescription we declare edges between targets and sources to be present in each region. We are going to look for closed paths in the wiring diagram of the brain, constructed from the non-zero entries $C(s_r, t_r)$ of the connection matrix. Direct approaches to persistent homology for asymmetric networks have been proposed, based on the Dowker complex, see [17], but the present doubling prescription takes advantage of the mesoscopic scale of the connectome data.

Given the family of $2R$ labelled vertices we have just described, we can construct a family of graphs and work out the families of independent loops for each of them by executing the following pseudo-code:

1. Consider a fixed $f \in]0, \max_{1 \leq r < s \leq R} d(r, s)]$ (referred to as a filtration value).
2. Draw an edge between any source labelled s_a and any target labelled t_b such that $d(s_a, t_b) \leq f$.
3. Work out generators of the homology groups $H_0(f)$ (connected components) and $H_1(f)$ (independent loops) in the resulting graph.

The family of graphs (depending on the parameter f) is called a simplicial complex. The third step of the procedure uses techniques of simplicial homology, implemented in JavaPlex [18, 19]. Simplices in our case consist of vertices (zero-simplices, corresponding to brain regions), and edges (one-simplices, corresponding to axons connecting two brain regions). The result of the above procedure depends on the value of the filtration value f . At $f = 0$ we have as many connected

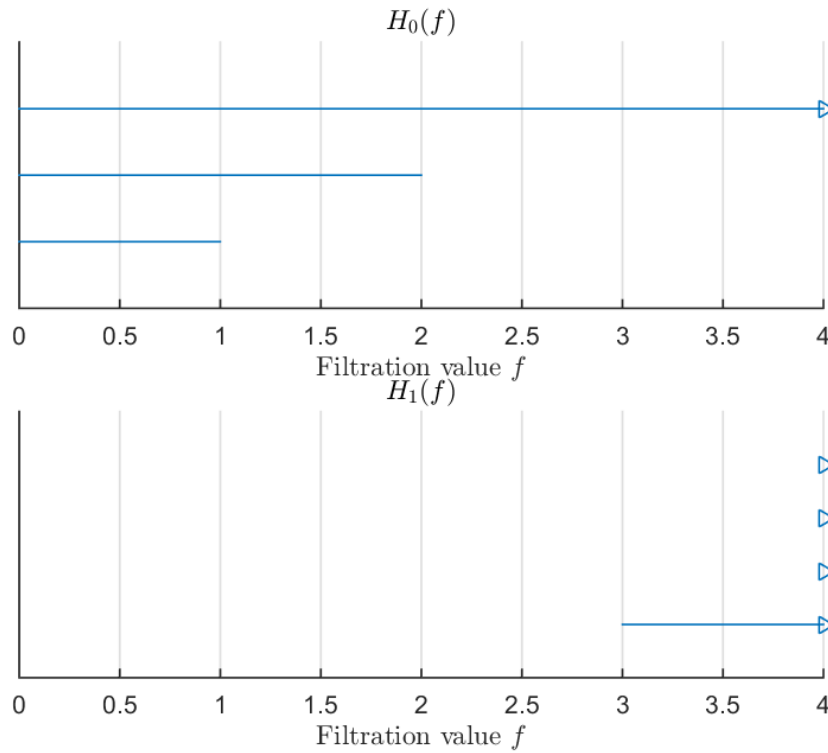
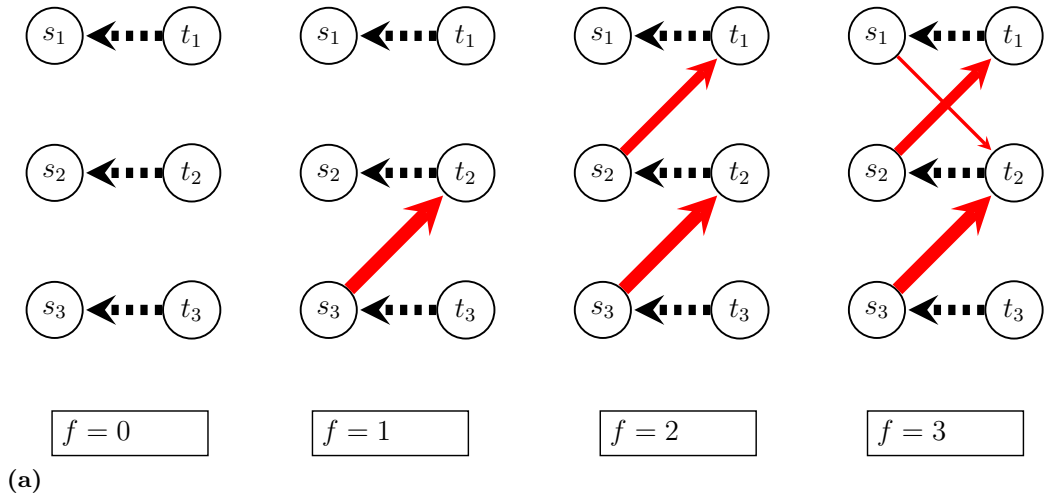


Fig 1. A toy model with three regions. (A) Each of the regions is doubled at filtration value zero, resulting in a source vertex and a target vertex. The filtered complex start with three connected components and no loop. For increasing using values of the filtration parameters, edges are drawn from to reflect projections from the nodes in the family $(s_r)_{1 \leq r \leq 3}$ to nodes in the family $(t_r)_{1 \leq r \leq 3}$. (B) The graph gets connected at filtration value $f = 2$ (resulting in $b_0(f) = 1$ for $f \geq 2$). A loop appears at $f = 3$, the corresponding generator of the first homology group is $[s_1, t_2] + [t_2, s_2] + [s_2, t_1] + [t_1, s_1]$. It goes through the regions labelled 1 and 2.

components as points, and no loop. The number of connected components decreases when f increases. It reaches 1 for some value of the filtration value. When f is increased beyond this value, edges may still be drawn, possibly changing the number of loops.

When f reaches the maximum entry of the matrix d , the simplicial complex cannot be changed anymore by increasing the filtration value. If we repeat the above procedure for all values of the entries of the matrix d , arranged in increasing order, we can work out for each feature F (which can be a connected component or a loop) an interval of filtration values $[f_{min}(F), f_{max}(F)]$ for which the feature F is present. These intervals can be drawn for all existing features F of a fixed dimension, yielding graphs of barcode form, one per dimension of feature (see Fig. 1B). Features persistent over a longer interval are thought less likely to be due to noise [20]. In particular, we will restrict ourselves to cycles that persist from their first appearance (at a given filtration value) to the maximum entry of the matrix d . The results of the above procedure are sketched of Fig. 1 for a toy model consisting of

three regions (and connection strengths assumed to be mapped to $d = \begin{pmatrix} 0 & 3 & 4 \\ 2 & 0 & 4 \\ 4 & 1 & 0 \end{pmatrix}$). The pseudo-code is executed for each unique value of the entries of d , in ascending order.

2.3 Neuroanatomy of cycles

2.3.1 Three-dimensional presentation of brain regions

To analyse the anatomy of persistent cycles, we used the voxelised version of the Allen Reference Atlas at a spatial resolution of 25 microns³. This three-dimensional grid contains numerical labels encoding neuroanatomy at the finest level compatible with the resolution (the voxelised atlas consists of $V_{tot} \simeq 3.1 \times 10^7$ cubic voxels, with 677 distinct regions). These numerical labels are associated to the names of brain regions according to the hierarchical annotation of the ARA⁴. For each of the $R = 213$ regions in the mesoscale model of the connectome (Eq. 1), we resolved the numerical label and the corresponding voxels. If the region has descendants in the hierarchical annotation, we lump together the voxels corresponding to these descendants, by annotating them with the numerical label of the region. After this step, the voxelised atlas contains 361 distinct regions. The regions included in the mesoscale model of the connectome therefore do not quite span the entire brain. Let us denote by V_r the number of voxels in region labelled r :

$$V_r = |\{v, \text{voxel labelled } v \in \text{region labelled } r\}|, \quad 1 \leq r \leq R. \quad (3)$$

The brain regions corresponding to the rows of the connectivity matrix contain

$$V = \sum_{r=1}^R V_r \simeq 2.4 \times 10^7 \text{ voxels}, \quad (4)$$

about 79 percent of the total volume V_{tot} of the brain. In the rest of this paper we will disregard the brain regions that are not included in the matrix of connectivity strengths, and the volume V will be referred to as the volume of the brain.

Grouping brain regions at a coarse hierarchical level (according to the ARA [3, 16]) yields the following major brain compartments which will sometimes be designated by acronyms for

³ See download instructions and code snippets in MATLAB and Python on the Allen Brain Atlas data portal: <http://help.brain-map.org/display/mouseconnectivity/API#API-DownloadAtlas3-DReferenceModels>

⁴The hierarchical system of annotation containing names of brain regions and numerical ids is available online at http://api.brain-map.org/api/v2/structure_graph_download/1.json

presentation purposes: Isocortex, olfactory areas (OLF), cortical subplate (CTXsp), striatum (STR), pallidum (PAL), thalamus (TH), hypothalamus (HY), midbrain (MB), medulla (MY), cerebellar cortex (CBX). These major brain compartments will be referred to as *big regions*.

2.3.2 Fraction of the brain connected by loops to a given region

Given a brain region labelled r and a filtration value f , let us denote by $\mathcal{C}_r(f)$ the family of generators of the first homology group at filtration value f that go through the region r :

$$\mathcal{C}_r(f) = \{c \in H_1(f), r \in c\}, \quad (5)$$

and by $\overline{\mathcal{C}_r(f)}$ the set of vertices through which the elements of $\mathcal{C}_r(f)$ go:

$$\overline{\mathcal{C}_r(f)} = \{s \in \{1, \dots, R\}, \exists c \in H_1(f), s \in c\}. \quad (6)$$

In the toy model of Fig. 1 with three brain regions, the sets $\mathcal{C}_1(2)$ and $\mathcal{C}_3(3)$ are empty. The set $\mathcal{C}_1(3)$ consists of one loop, corresponding to $\overline{\mathcal{C}_1(3)} = \{1, 2\}$.

We can calculate the volume of the regions connected to the region r by loops, as a fraction of the total number of voxels in the brain:

$$\phi_r(f) = \frac{1}{V} \sum_{s \in \overline{\mathcal{C}_r(f)}} V_s. \quad (7)$$

where V is the total number of voxels defined in Eq. 4, and V_s is the number of voxels in region labelled s . As the volumes of brain regions are not all equal, we can define an alternative measure by the fraction of the total number of regions connected to region labelled r by loops:

$$\nu_r(f) = \frac{1}{R} |\overline{\mathcal{C}_r(f)}|. \quad (8)$$

For a region labelled r that is connected by loops to all brain regions, for some value of the filtration f , we will have $\phi_r(f) = \nu_r(f) = 1$.

It is natural to compare these ratios to the analogous ratios obtained by taking into account only direct connections between pairs of brain regions, as encoded by the connectivity matrix C . Let us denote these quantities by $\phi_r^{(c)}(f)$ for the fraction of volume and by $\nu_r^{(c)}(f)$ for the fraction of the number of regions:

$$\phi_r^{(c)}(f) = \frac{1}{V} \sum_{s=1}^R V_s \max(\mathbf{1}(C(r, s) > f), \mathbf{1}(C(s, r) > f)), \quad (9)$$

$$\nu_r^{(c)}(f) = \frac{1}{R} \sum_{s=1}^R \max(\mathbf{1}(C(r, s) > f), \mathbf{1}(C(s, r) > f)), \quad (10)$$

where $\mathbf{1}$ denotes the indicator function. By construction the four fractions defined in Eqs 7,8,9,10 are growing functions of the filtration value f . There can be regions in the family $\overline{\mathcal{C}_r(f)}$ that are not directly connected to region r based on the inter-region connectivity matrix. There can also be regions with projections to or from region r that are not involved in any closed cycle going through region r at the given filtration value f . There is therefore no a priori solidarity between the quantities ϕ and ν , based on loops, and their analogues $\phi^{(c)}$ and $\nu^{(c)}$, based on direct connections.

2.4 Brain-wide maps of loops going through a given brain region

To sum up the connections by loops between two given brain regions, we can calculate the sum of connection strengths at which cycles connecting these two regions appear, weighted by the numbers of such cycles. As the generators of the first homology groups are independent, this is consistent with the additivity assumption of connection strengths between brain regions. For two regions labelled r and s we introduce

$$\omega(r, s) = \sum_f e^{-f} \mathbf{1}(s \in \overline{\mathcal{C}_r(f)}), \quad (11)$$

where the sum is over the distinct filtration values (the distinct entries of the matrix d defined in Eq. 2), and the exponential function comes from Eq. 2 relating connection strengths to the distance used to defined filtration values.

Fixing the region label r and allowing the region label s to take all the possible values in $\{1, \dots, R\}$, we can define a brain-wide map of connection strengths to region labelled r , by defining for voxel labelled v :

$$\mathcal{W}_r(v) = \sum_f e^{-f} \mathbf{1}(s(v) \in \overline{\mathcal{C}_r(f)}), \quad (12)$$

where $s(v)$ is the index (in $\{1, \dots, R\}$) of the brain region to which voxel labelled v belongs. The quantity \mathcal{W}_r maps a voxel to a real number, and can be visualised as a heat map for instance.

To estimate how localised a brain-wide map of connection strengths is, we can compute the Kullback–Leibler divergence from the above-defined profile and the uniform brain-wide density. If we denote by the label of the region to which voxel labelled v belongs, this divergence is expressed as

$$KL(r) = \frac{1}{V} \sum_{v=1}^V \mathcal{W}_r(v) \log(\mathcal{W}_r(v)), \quad (13)$$

where V is the total number of voxels defined in Eq. 4, and we used the fact that \mathcal{W}_r/V is a normalised density function. This divergence induces a ranking of brain regions.

3 Results

3.1 Persistent cycles

The bar code corresponding to the persistent generators of the first two homology groups is shown in Fig. 2. The maximum Betti numbers are too large for the individual bars to be visible, as they are on Fig. 1B. By construction the Betti number b_0 starts at $R = 213$. The Betti number b_1 starts at 0 and the plateau at filtration value 25 in the bar code of the first homology group corresponds to $b_1 = 16,529$. At filtration values larger than $f_{conn} = 7$, all brain regions are in the same connected component. Moreover, from the growth profile of the bar code of the first homology group, we can see that thousands of persistent cycles appear at filtration values lower than f_{conn} ($b_1 = 8,230$ at $f = f_{conn}$).

3.2 Loops highlight the cortico-striato-thalamic network

To obtain a coarse picture of the anatomy of cycles, let us work out which family of *big regions* (as defined in Section 2.3.1) is intersected by each loop. We can rank the resulting families of big regions by decreasing value of prevalence. For an example of the brain regions in a loop appearing at filtration

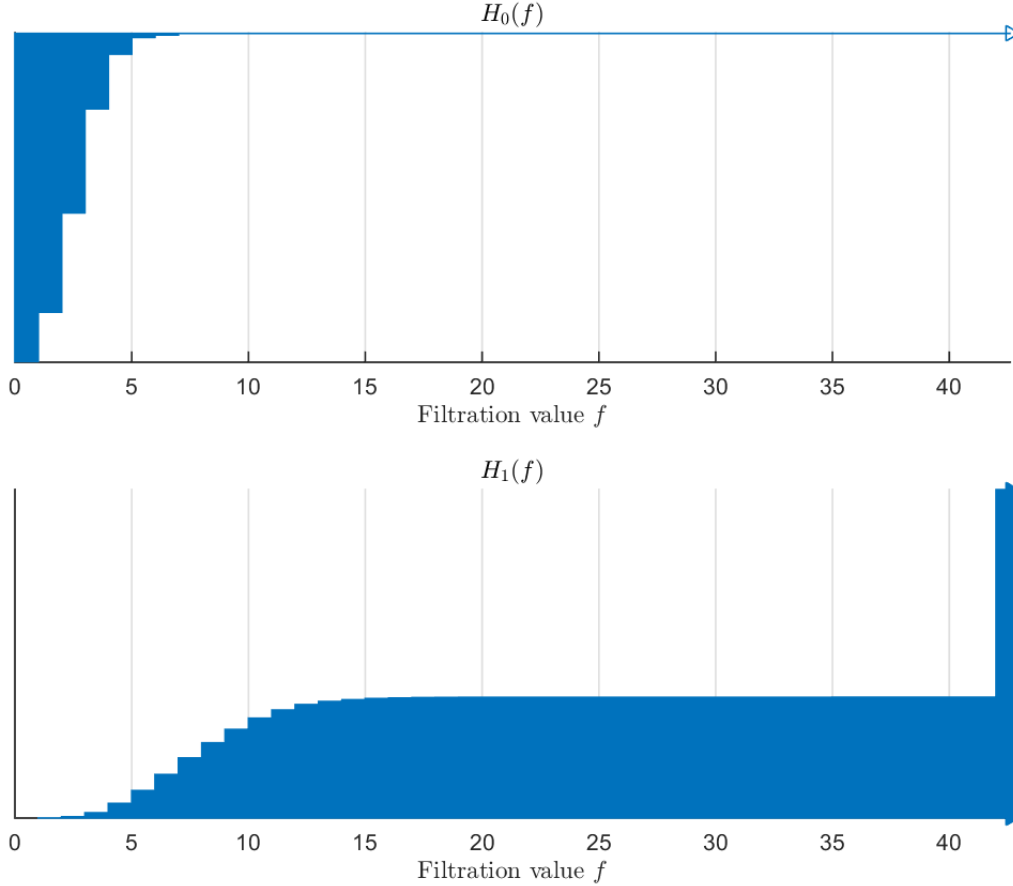


Fig 2. Bar code of the complex based on the inter-region connectivity matrix. The second plateau that appears at filtration value $f = 42$ corresponds to $-\log \epsilon$, where ϵ is the regulator introduced in Eq. 2. The shape of the barcode and the families of generators of H_1 and H_0 would be unchanged if ϵ went to zero.

value $f = 2$, together with the names of the corresponding big regions, see Table 1. This loop appears at a low filtration value and we will see that the family of big regions it intersects (isocortex, striatum, thalamus and midbrain) is frequent among loops in the wiring diagram of the mouse brain.

For definiteness we did this calculation at two special filtration values:

- the filtration value $f_{conn} = 7$ at which the Betti number b_0 falls to 1.
- the maximum filtration value ($f_{max} = 37$), above which no extra loops appear (before the value $-\log \epsilon = 42$ introduced in Eq. 2 to provide a cut-off to the plots).

We found that 334 distinct families of big regions occur, but the most frequent 27 families account for 50% of the loops. The most prevalent families of big regions are presented in Table 2 (where they are ordered by decreasing prevalence at filtration value $f = 7$). We notice that midbrain is represented in most of the rows of this table⁵, and that the three most frequent combinations (accounting for more than 10% of all the loops) go through six or more big regions. The family of four big regions corresponding to the regions in the loop presented in Table 1 is the fourth most

⁵Midbrain is also represented in most of the loops that appear at low filtration values $f < 3$.

Table 1. Brain regions in a circuit appearing at filtration value $f = 2$.

Brain region	Big region
Anterior cingulate area, dorsal part	Isocortex
Primary auditory area	Isocortex
Caudoputamen	Striatum
Medial geniculate complex, dorsal part	Thalamus
Medial geniculate complex, ventral part	Thalamus
Superior colliculus, motor related	Midbrain

Six regions appear, belonging to four distinct *big* brain regions.

prevalent family of big regions in loops appearing at filtration values lower than $f = 7$, with 249 distinct loops (resp. fifth, $f = 37$ and 328 loops). If we focus on small families of big regions (with three regions or fewer), we observe that the most prevalent is the cortico-striato-thalamic family (7th row of the table, with 183 loops at $f = 7$). Highlighting occurrences of isocortex, striatum and thalamus in colour in Table 1 (in red, green and blue respectively), we notice that the first 17 rows present at least one of these colours (in 14 cases associated with midbrain, highlighted in brown). The next small family consists of isocortex and striatum (16th rank, with 106 loops), followed at rank 18 by medulla. With 104 loops, medulla contains more cycles than the cortico-thalamic family (ranked 25 with 80 loops). Moreover, medulla is the only single big region to support more than 10 cycles (see Table 3, which shows that only 147 cycles are confined to a single big region, out of which 134 appear before the filtration value 7).

To assess whether the dominance of medullar loops among loops confined to a single big region could have been guessed based on the matrix of connectivity strengths, let us calculate how much of the connection strengths from its sub-regions project within the same region. For each big region labelled b , let us define:

$$\frac{C_{intra}}{C_{tot}}(b) = \frac{\sum_{r=1}^R \sum_{s=1}^R \mathbf{1}(B(r) = b)\mathbf{1}(B(s) = b)C(r, s)}{\sum_{r=1}^R \sum_{s=1}^R \mathbf{1}(B(r) = b)C(r, s)}, \quad (14)$$

where the symbol $\mathbf{1}(B(r) = b)$ equals 1 if the region labelled r is part of the big region labelled b (for instance we can read from the third row of Table 1 that $\mathbf{1}(B(\text{Caudoputamen}) = \text{Striatum}) = 1$). The ratio C_{intra}/C_{tot} is the conditional probability of a connection from within the big region b to project within region b . The sorted values of this ratio are plotted on Fig. 3. The average value is 31%, and the values range from 6% (thalamus) to 68% (cerebellar cortex, which is found to contain only one loop, see Table 3B).

The fact that 80 percent of the cycles confined to a single big region are in medulla could not have been guessed based on the connectivity matrix only: 47% of connections from medullar regions project to medullar regions, which is above average, but the medulla is only ranked fourth among 12 big regions by our measure of conditional probability.

3.3 Loops can connect brain regions to the entire brain

On average, loops connect a given brain region to a larger domain in the brain than direct projections. This is true for both the volumetric and the counting measures defined in Eqs 9 and 10, and at all filtration values. This can be observed on Fig. 4, where the following averages across all

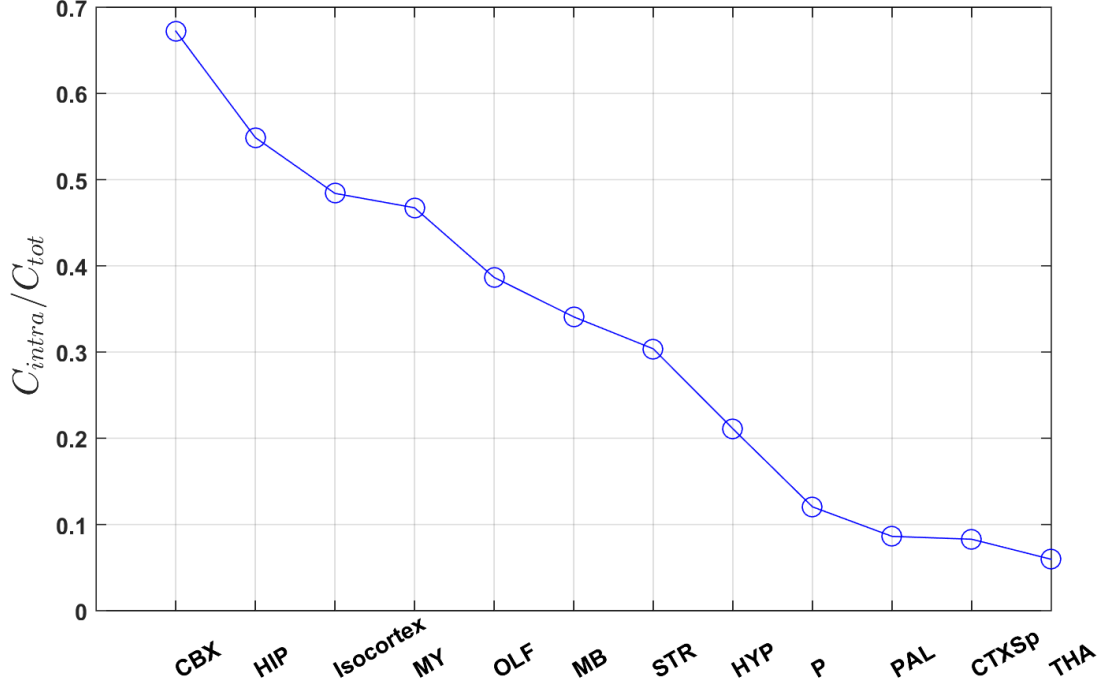


Fig 3. Fraction of inter-region connection strengths supported in the big region of origin. Acronyms of big regions read as follows: OLF = olfactory areas, HPF = hippocampal formation, CTXsp = cortical subplate, STR = striatum, PAL = pallidum, TH = thalamus, HY = hypothalamus, MB = midbrain, MY = medulla, CBX = cerebellar cortex.

brain regions are plotted:

$$\begin{aligned}
 \langle \phi(f) \rangle &:= \frac{1}{R} \sum_{i=1}^R \phi_r(f), & \langle \nu(f) \rangle &= \frac{1}{R} \sum_{i=1}^R \nu_r(f), \\
 \langle \phi^{(c)}(f) \rangle &= \frac{1}{R} \sum_{i=1}^R \phi_r^{(c)}(f), & \langle \nu^{(c)}(f) \rangle &= \frac{1}{R} \sum_{i=1}^R \nu_r^{(c)}(f).
 \end{aligned} \tag{15}$$

Moreover, all four averages reach an asymptote, and the ratios of asymptotic values do not depend heavily on the choice of measure, as:

$$\langle \phi(25) \rangle \simeq 1.39 \langle \phi^{(c)}(25) \rangle \simeq 87\%, \quad \text{and} \quad \langle \nu(25) \rangle \simeq 1.37 \langle \nu^{(c)}(25) \rangle \simeq 80\%. \tag{16}$$

However, the maximum values of the fractions ϕ_r and ν_r are highly heterogeneous among brain regions. The heat map of Fig. 5 shows the fraction of the brain $\phi_r(f)$, with the region labels r grouped by big regions (and ordered within each big region by decreasing value of the maximum reached at large filtration value). In particular, 18 regions reach the entire brain through connections by loops. Their names are shown on Table 4, together with the big regions to which they belong (midbrain is the most represented big region, with 4 regions). The ansiform lobule, which is part of the cerebellar cortex, is connected to the entire brain by loops, and is the brain region connected to the largest volume in the brain based on the connectivity matrix (it is ranked first by the measure

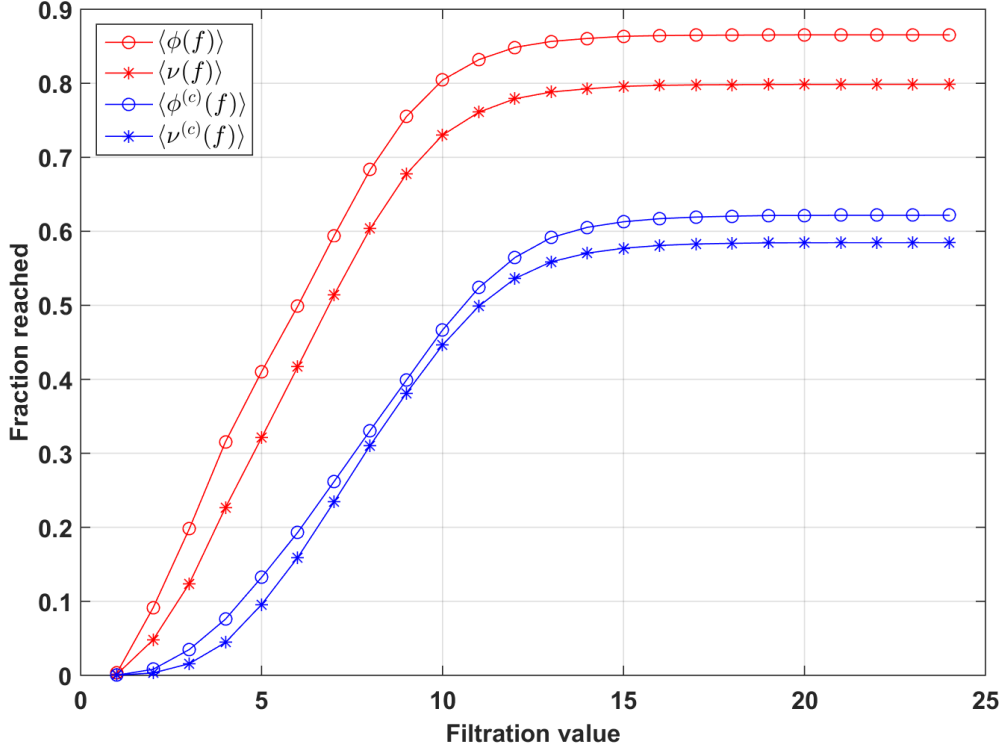


Fig 4. Fraction of the brain reached by loops, averaged across all regions in the connectivity atlas.

$\phi^{(c)}$). However, not all the regions appearing in Table 4 are that strongly connected based on the connectivity matrix. For instance the posterior amygdalar nucleus is ranked 173 out of 213 by the measure $\psi^{(c)}$.

3.4 Brain-wide density of connections by loops to a given region

The region for which W_r has lowest Kullback–Leibler divergence from a uniform profile is the nucleus accumbens. The region with highest Kullback–Leibler divergence from a uniform profile is the flocculus, a region in the cerebellar cortex. Heat maps of the densities of loops for both regions are shown on Fig. 6. They are projected on sagittal, coronal and axial planes. For each of these regions the volume can be presented either as the sum of values of voxels (Figs 6A,C) or as maximal-intensity projections (Figs 6B,D). On maximal-intensity projections of the density W_r , the voxels belonging to region labelled r have the largest value by construction (because all loops go through this region). Maximal-intensity projections can exhibit at most R different values (they are piecewise constant on each brain region). On the other hand, projections of sums of the density W_r may have higher values in voxels that do not belong to region labelled r , depending on the direction of projection. Even though nucleus accumbens is connected to the entire brain by loops (meaning all the voxels in Figs. 6A,B correspond to non-zero values), the plots still appear rather shallow, and the strength of connection by loops is still far from uniform, even in the region that minimises the divergence from a uniform brain-wide profile.

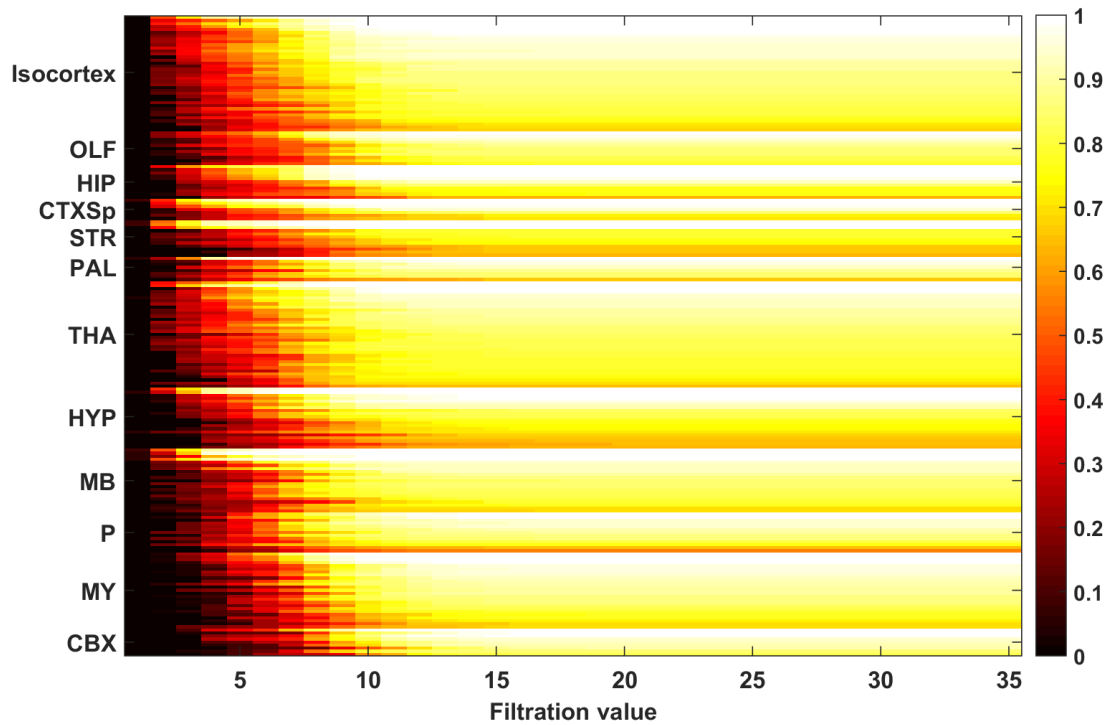


Fig 5. Heat maps of the fraction of the brain reached by loops $\phi_r(f)$, as a function of the filtration value (horizontal axis). The rows correspond to brain regions (grouped by big regions according to coarse neuroanatomy). The subregions in each big region are ordered by decreasing value of the asymptote $\phi_r(35)$.

Table 2. Families of big regions containing loops.

Rank (out of 334)	Number of loops ($f = 7$)	Cumulated percent- age of loops ($f = 7$)	Number of loops ($f = 37$)	Cumulated percent- age of loops ($f = 37$)	Big regions intersected
1	410	6%	600	4%	Cortical Subplate, Hippocampal Formation, Hypothalamus, Isocortex , Midbrain , Striatum , Thalamus
2	268	9%	614	8%	Cortical Subplate, Hypothalamus, Isocortex , Midbrain , Striatum , Thalamus
3	265	12%	455	11%	Cortical Subplate, Hypothalamus, Isocortex , Midbrain , Pallidum, Striatum , Thalamus
4	249	15%	328	13%	Isocortex , Midbrain , Striatum , Thalamus
5	248	19%	346	15%	Hypothalamus, Isocortex , Midbrain , Pallidum, Striatum , Thalamus
6	199	21%	283	17%	Hypothalamus, Isocortex , Midbrain , Striatum , Thalamus
7	183	23%	222	19%	Isocortex , Striatum , Thalamus
8	165	25%	255	20%	Cortical Subplate, Isocortex , Midbrain , Striatum , Thalamus
9	141	27%	175	21%	Hypothalamus, Isocortex , Midbrain , Thalamus
10	135	29%	175	22%	Hypothalamus, Midbrain , Pallidum, Thalamus
11	130	31%	190	24%	Cortical Subplate, Hippocampal Formation, Hypothalamus, Midbrain , Striatum , Thalamus
12	130	32%	208	25%	Cortical Subplate, Hippocampal Formation, Hypothalamus, Isocortex , Midbrain , Pallidum, Striatum , Thalamus
13	122	34%	149	26%	Cortical Subplate, Isocortex , Striatum
14	115	35%	163	27%	Hypothalamus, Isocortex , Midbrain , Pallidum, Thalamus
15	107	37%	135	28%	Cortical Subplate, Hypothalamus, Isocortex , Midbrain , Pallidum, Striatum
16	106	38%	117	29%	Isocortex , Striatum
17	105	39%	139	29%	Cortical Subplate, Hippocampal Formation, Hypothalamus, Midbrain , Olfactory Areas, Striatum , Thalamus
18	104	40%	115	30%	Medulla
19	96	42%	108	31%	Hypothalamus, Midbrain , Thalamus
20	85	43%	104	32%	Hypothalamus, Midbrain , Pallidum
21	85	44%	111	32%	Hypothalamus, Isocortex , Midbrain , Pallidum, Striatum
22	84	45%	118	33%	Medulla , Midbrain , Pallidum

The families of big regions are ordered by decreasing number of loops they contain (at filtration value $f = 7$).

Table 3. Tables of single big regions containing loops, ordered by decreasing number of loops.

Number of loops	Fraction (%)	Big region label
104	78	Medulla
8	6	Hippocampal Formation
8	6	Hypothalamus
6	5	Olfactory Areas
5	4	Isocortex
3	3	Midbrain

(A)

Number of loops	Fraction (%)	Big region label
115	79	Medulla
9	7	Hypothalamus
8	6	Hippocampal Formation
6	5	Olfactory Areas
5	4	Isocortex
3	3	Midbrain
1	1	Cerebellar Cortex

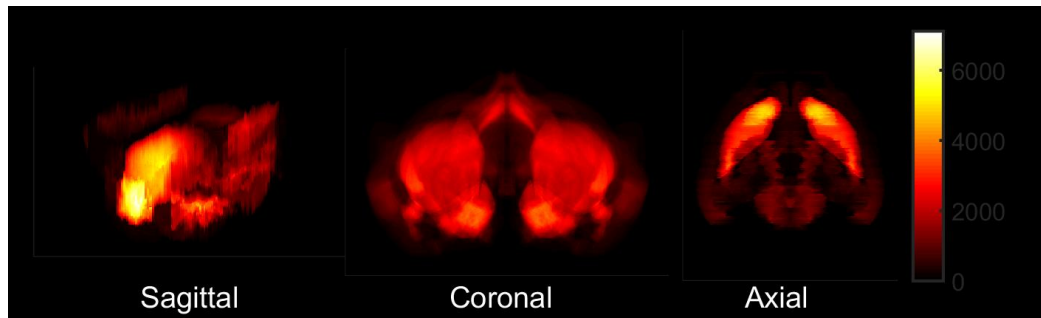
(B)

(A) For filtration value $f = 7$, there is a total of 134 cycles. (B) For filtration value $f = 37$, there are 147 loops, and just one more region represented.

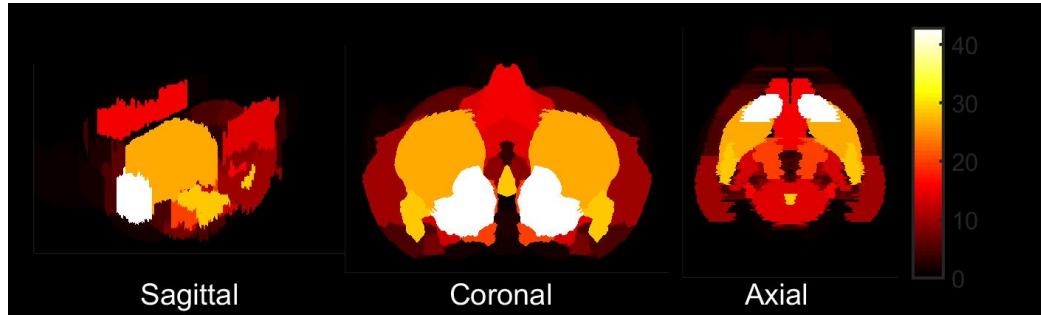
Table 4. Table of brain regions connected to all brain regions by loops.

Big region	Name of region	$\phi_r^{(c)}(25)(\%)$	Rank by $\phi^{(c)}$, out of 213
Isocortex	Anterior cingulate area, dorsal part	85	13
Hippocampal Formation	Entorhinal area, lateral part	81	31
Cortical Subplate	Basolateral amygdalar nucleus	81	29
Cortical Subplate	Posterior amygdalar nucleus	50	173
Striatum	Nucleus accumbens	68	73
Striatum	Caudoputamen	55	148
Striatum	Medial amygdalar nucleus	59	123
Pallidum	Globus pallidus, internal segment	77	40
Thalamus	Medial geniculate complex, dorsal part	71	64
Thalamus	Peripeduncular nucleus	74	52
Hypothalamus	Lateral hypothalamic area	70	67
Hypothalamus	Subthalamic nucleus	73	56
Midbrain	Central linear nucleus raphe	75	49
Midbrain	Midbrain reticular nucleus	56	138
Midbrain	Periaqueductal gray	66	87
Midbrain	Superior colliculus, motor related	59	125
Cerebellar Cortex	Ansiform lobule	98	1

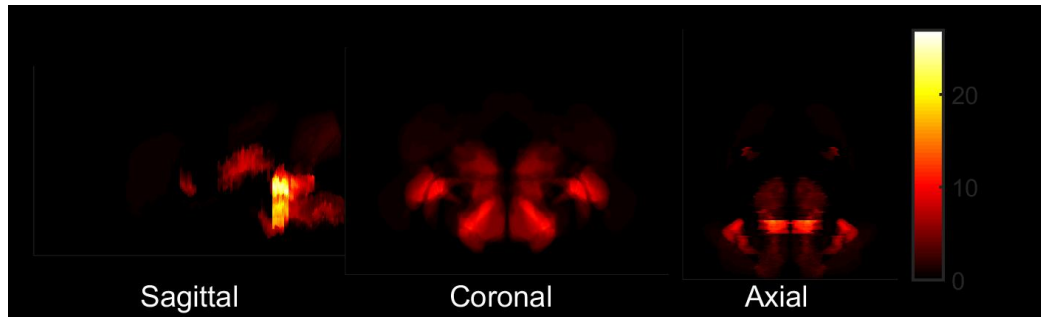
On average these brain regions are connected to 72% of the volume of the brain by direct connections, which is largest than the average value $\langle \phi^{(c)} \rangle \simeq 63\%$. However, 5 regions correspond to values below this average.



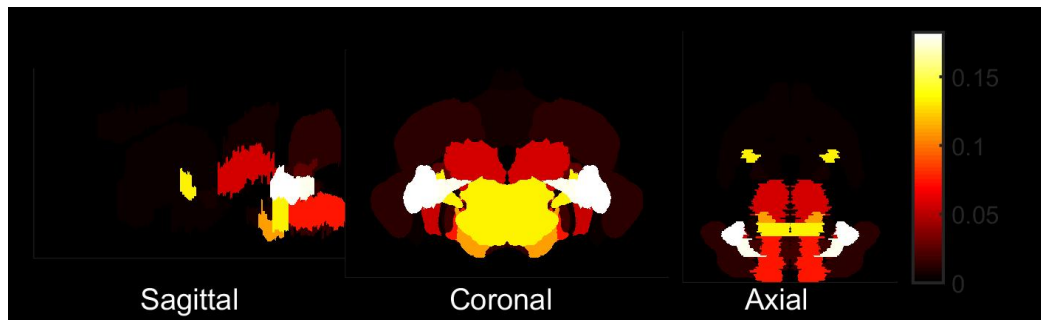
(a)



(b)



(c)



(d)

Fig 6. Heat map of the weighted regions connected by loops to given brain regions, projected in the sagittal, coronal and axial directions. (A) Nucleus accumbens, projection of sums of intensities. (B) Nucleus accumbens, projection of maximal intensities. (C) Flocculus, projection of sums of intensities. (D) Flocculus, projection of maximal intensities. For visualisation purposes, both hemispheres are shown, even though the results are based on the ipsilateral connectivity matrix only.

4 Discussion

Persistent homology reveals global properties of the mouse connectome at the mesoscopic scale. The high prevalence of cortico-striato-thalamic loops is a strong consistency check between the mesoscale experimental approach [1, 2] and the present topological method, as the cortico-striato-thalamo-cortical circuit is known as a major circuit regulating complex behaviours (for a review of its involvement in the Tourette syndrome see [21]).

The global nature of topological tools reveals connections between regions that are not linked by direct projections. Moreover, the lists of generators of the first homology groups allow to count the number of independent loops for a given threshold in connection strengths. The relative abundance of closed loops in the medulla is perhaps best interpreted in terms of the life-sustaining automatic functions regulated by the medulla. The corresponding circuits are topologically insulated from circuits involved in conscious behaviours or learning [22].

Axons, in addition to conducting action potentials, transport biological molecules [23, 24]. Integration with other brain-wide data sets, in particular gene-expression data [25, 26], has already shown that connected regions in the adult rodent brain have increased similarity in gene-expression profiles, and sets of genes most correlated to connectivity have been identified (see [27] for results based on connectivity data in the rat brain). It would be interesting to investigate to which extent these correlations persist across the loops that we identified in the mouse brain. Moreover, spatial gene expression patterns have been related to cortico-striatal functional networks [28]. Loops that are as persistent as the cortico-striatal ones yield natural candidates for places where to look for such genetic signatures of functional networks. Moreover, the brain-wide coverage of the gene-expression atlas [25, 26] allows to estimate spatial densities of cell types known by their transcriptional activity [29, 30, 33], which yields neuroanatomical predictions relevant to brain disorders [31, 32]. The present work could lead to insights into the correlation structure between the local density of loops and the spatial density of cell types. Another direction of research is the conservation of patterns across species [34–36], even though gene-expression and connectivity data do not have the same brain coverage as in the mouse atlas.

We have worked out the persistent loops of the wiring diagram of the brain based on ipsilateral projections only, leaving out the issue of contralateral projections. Contralateral projections have been mapped (see [1], right-hand side of Fig. 4A), but they do not allow to work out closed loops because the missing projections would involve injecting tracers into the left hemisphere, and mapping the contralateral projections again. However, the known contralateral connection strengths have been found to be significantly weaker than ipsilateral ones. One can therefore conjecture that loops going through brain regions in different hemispheres do not dramatically change the global features of the wiring diagram of the brain.

There are surprisingly few cycles confined to only one of the major brain regions (or big regions), but most of them develop before the brain becomes fully connected. Moreover, medulla is by far the region with the most confined loops.

5 Acknowledgments

This work is supported by the Research Center for Precision Medicine, HT-URC, Xi'an Jiaotong-Liverpool University, Suzhou, China.

References

1. Oh SW, Harris J, Ng L, Winslow B, Cain N, Mihalas S, et al. A mesoscale connectome of the mouse brain. *Nature*. Nature Publishing Group; 2014;508: 207–14. pmid:24695228.
2. Bohland JW, Wu C, Barbas H, Bokil H, Bota M, Breiter H C, et al. A proposal for a coordinated effort for the determination of brainwide neuroanatomical connectivity in model organisms at a mesoscopic scale. 2009; *PLoS computational biology*, 5(3), e1000334.
3. Dong HW . The Allen reference atlas: A digital color brain atlas of the C57Bl/6J male mouse. John Wiley & Sons Inc; 2009.
4. Barabási AL, Albert R. Emergence of scaling in random networks. 1999; *Science*, 286(5439), 509–512.
5. Watts DJ, Strogatz SH. Collective dynamics of ‘small-world’ networks. *Nature*. 1998 Jun;393(6684):440.
6. Edelsbrunner H, Letscher D, Zomorodian A. Topological persistence and simplification. In *Foundations of Computer Science*, 2000. Proceedings. 41st Annual Symposium on 2000 (pp. 454-463). IEEE.
7. Edelsbrunner H, Harer J. *Computational topology: an introduction*. American Mathematical Soc.; 2010.
8. Zomorodian A, Carlsson G. Computing persistent homology. *Discrete & Computational Geometry*. 2005 Feb 1;33(2):249–74.
9. Wasserman L. Topological data analysis. *Annual Review of Statistics and Its Application*. 2018 Mar 7;5:501–32.
10. Chan JM, Carlsson G, Rabadan R. Topology of viral evolution. *Proceedings of the National Academy of Sciences*. 2013 Oct 29;201313480.
11. Curto C, Giusti C, Marku K, Pastalkova E, Itskov V. Pairwise correlation graphs from hippocampal population activity have highly non-random, low-dimensional clique topology. *BMC neuroscience*. 2013 Jul;14(1):P182.
12. Petri G, Expert P, Turkheimer F, Carhart-Harris R, Nutt D, Hellyer PJ, Vaccarino F. Homological scaffolds of brain functional networks. *Journal of The Royal Society Interface*. 2014 Dec 6;11(101):20140873.
13. Giusti C, Pastalkova E, Curto C, Itskov V. Clique topology reveals intrinsic geometric structure in neural correlations. *Proceedings of the National Academy of Sciences*. 2015 Nov 3;112(44):13455-60.
14. Sizemore AE, Giusti C, Kahn A, Vettel JM, Betzel RF, Bassett DS. Cliques and cavities in the human connectome. *Journal of computational neuroscience*. 2018 Feb 1;44(1):115-45.
15. Saggar M, Sporns O, Gonzalez-Castillo J, Bandettini PA, Carlsson G, Glover G, Reiss AL (2018). Towards a new approach to reveal dynamical organization of the brain using topological data analysis. *Nature communications*, 9(1), 1399.

16. Swanson L (2004). Brain maps: structure of the rat brain. Gulf Professional Publishing.
17. Chowdhury S, Mémoli F (2018). A functorial Dowker theorem and persistent homology of asymmetric networks. *Journal of Applied and Computational Topology*, 2(1-2), 115–175.
18. Adams H, Tausz A, Vejdemo-Johansson M (2014, August). JavaPlex: A research software package for persistent (co) homology. In *International Congress on Mathematical Software* (pp. 129–136). Springer, Berlin, Heidelberg.
19. Adams H, Tausz A, *JavaPlex tutorial*, available from http://www.math.duke.edu/~hadams/research/javaplex_tutorial.pdf
20. Collins A, Zomorodian A, Carlsson G, Guibas LJ (2004). A barcode shape descriptor for curve point cloud data. *Computers & Graphics*, 28(6), 881–894.
21. Robertson MM, Eapen V, Singer HS, Martino D, Scharf JM, Paschou P, et al. (2017). Gilles de la Tourette syndrome. *Nature reviews Disease primers*, 3, 16097.
22. Rybak IA, Shevtsova NA, Paton JFR, Dick TE, John WS, Mörschel M, et al. (2004). Modeling the ponto-medullary respiratory network. *Respiratory physiology & neurobiology*, 143(2-3), 307–319.
23. Paus T, Pesaresi M, French L (2014). White matter as a transport system. *Neuroscience*, 276, 117–125.
24. Josh Huang Z, Zeng H (2013). Genetic approaches to neural circuits in the mouse. *Annual review of neuroscience*, 36, 183-215.
25. Lein ES, Hawrylycz MJ, Ao N, Ayres M, Bensinger A, Bernard A, Boe AF, Boguski MS, Brockway KS, Byrnes EJ, Chen L. Genome-wide atlas of gene expression in the adult mouse brain. *Nature*. 2007 Jan;445(7124):168.
26. Ng L, Bernard A, Lau C, Overly CC, Dong HW, Kuan C, Pathak S, Sunkin SM, Dang C, Bohland JW, Bokil H. An anatomic gene expression atlas of the adult mouse brain. *Nature neuroscience*. 2009 Mar;12(3):356.
27. French L, Pavlidis P. Relationships between gene expression and brain wiring in the adult rodent brain. *PLoS computational biology*. 2011 Jan 6;7(1):e1001049.
28. Anderson KM, Krienen FM, Choi EY, Reinen JM, Yeo BT, Holmes AJ. Gene expression links functional networks across cortex and striatum. *Nature communications*. 2018 Apr 12;9(1):1428.
29. Grange P, Bohland JW, Okaty BW, Sugino K, Bokil H, Nelson SB, Ng L, Hawrylycz M, Mitra PP. Cell-type-based model explaining coexpression patterns of genes in the brain. *Proceedings of the National Academy of Sciences*. 2014 Mar 25;201312098.
30. Grange P, Hawrylycz M, Mitra PP. Computational neuroanatomy and co-expression of genes in the adult mouse brain, analysis tools for the Allen Brain Atlas. *Quantitative Biology*. 2013 Mar 1;1(1):91–100.
31. Menashe I, Grange P, Larsen EC, Banerjee-Basu S, Mitra PP. Co-expression profiling of autism genes in the mouse brain. *PLoS computational biology*. 2013 Jul 25;9(7):e1003128.

32. Grange P, Menashe I, Hawrylycz M. Cell-type-specific neuroanatomy of cliques of autism-related genes in the mouse brain. *Frontiers in computational neuroscience*. 2015 May 29;9:55.
33. Bohland JW, Bokil H, Pathak SD, Lee CK, Ng L, Lau C, Kuan C, Hawrylycz M, Mitra PP. Clustering of spatial gene expression patterns in the mouse brain and comparison with classical neuroanatomy. *Methods*. 2010 Feb 1;50(2):105-12.
34. Sporns O. The human connectome: a complex network. *Annals of the New York Academy of Sciences*. 2011 Apr;1224(1):109-25.
35. Stafford JM, Jarrett BR, Miranda-Dominguez O, Mills BD, Cain N, Mihalas S, Lahvis GP, Lattal KM, Mitchell SH, David SV, Fryer JD. Large-scale topology and the default mode network in the mouse connectome. *Proceedings of the National Academy of Sciences*. 2014 Dec 30;111(52):18745-50.
36. Hawrylycz M, Miller JA, Menon V, Feng D, Dolbeare T, Guillozet-Bongaarts AL, et al. Canonical genetic signatures of the adult human brain. *Nat Neurosci*. Nature Publishing Group, a division of Macmillan Publishers Limited. All Rights Reserved.; 2015;18: 1832–1844.